

Zero- \bar{n} bandgap in photonic crystal superlattices

Nicolae C. Panoiu and Richard M. Osgood, Jr.

Department of Applied Physics and Applied Mathematics, Columbia University, New York, New York 10027

Shuang Zhang and Steven R. J. Brueck

Center for High Technology Materials and Department of Electrical and Computer Engineering, University of New Mexico, Albuquerque, New Mexico 87106

Received July 8, 2005; revised October 5, 2005; accepted October 7, 2005; posted October 12, 2005 (Doc. ID 63335)

We demonstrate that photonic superlattices consisting of a periodic distribution of layers of materials with positive index of refraction and photonic crystal slabs that, at the operating frequency, have negative effective index of refraction present a photonic gap that corresponds to the frequency at which the spatial average of the refractive index distribution, taken over the unit supercell of the superlattice, vanishes. We also show that, unlike the Bragg gaps, the frequency of this zero- \bar{n} gap is invariant to the geometrical scaling of the superlattice or the direction of wave propagation in the superlattice. © 2006 Optical Society of America
OCIS codes: 230.4170, 130.3120, 160.3130, 260.2110.

1. INTRODUCTION

Left-handed metamaterials (LHMs) are newly discovered artificial composites,^{1–3} which have attracted much interest over the past few years. Their main physical property is that both the electric permittivity ϵ and the magnetic permeability μ are negative; as a result, they also have a negative index of refraction. Although the main electromagnetic properties of a medium with such characteristics have been theoretically investigated more than three decades ago,⁴ the lack of naturally occurring media with simultaneously negative ϵ and μ has made it impossible to experimentally verify the striking predictions of this theoretical study. However, it has been recently demonstrated that it is possible to achieve both negative ϵ and μ , within a certain frequency domain, if metallic periodically structured composites are used. Thus, it has been shown that a network of thin metallic wires behaves as a quasi medium with negative ϵ ,^{5,6} whereas a lattice of metallic split-ring resonators has a negative μ .⁷ Combining these two structures leads to a LHM.^{1–3} Alternative designs of the metal-based LHM have been proposed and recently demonstrated.^{8,9}

The rapidly growing interest in LHMs stems from their unusual physical properties, such as superlensing,^{10–12} an inverse Snell's law,⁴ or an inverse Doppler effect,⁴ as well as from their potential use in new technological applications. In addition, metal-based LHMs can operate not only at microwave frequencies, as several studies have initially demonstrated,^{1–3} but, as recent theoretical^{13–15} and experimental⁹ investigations have shown, also at infrared and optical frequencies. A main drawback of using metal-based LHMs for optical devices is their large losses, which are mainly due to the optical losses in their metallic components. One way to overcome this limitation is to use periodically structured dielectrics, namely, photonic crystals (PCs). Thus, it has been recently demonstrated^{16–19} that, within a certain frequency range,

PCs behave like materials with negative index of refraction: the incident and transmitted waves lie on the same side of the normal to the interface,^{16,17,20} so that the effective index of refraction is negative; a slab of PC behaves like a lens and produces a real image of a point source placed in front of the slab²¹; or the PC can be used to achieve subwavelength resolution.^{22,23}

In the case of a PC-based LHM, the background matrix is usually made from a homogeneous nonmagnetic ($\mu = 1$) dielectric material. In this case, the property of negative effective index of refraction is a direct consequence of the spatial periodicity of the dielectric function; i.e., it is the effect of modified dispersive properties induced by folding the photonic bands back into the first Brillouin zone. Furthermore, alternating layers of homogeneous LHMs and right-handed materials (RHMs), i.e., regular dielectric materials with positive ϵ and μ , can be combined in a periodic photonic superlattice that shows remarkable optical properties.^{24,25} The presence of the LHM component in these periodic structures leads to surprising effects, such as the existence of an omnidirectional bandgap that is insensitive to the wave polarization, angle of incidence, or period of the structure,²⁶ and unusual transmission properties and beam reshaping.^{27,28} As has been shown, the main reason for such remarkable properties is the existence of a frequency at which the volume-averaged refractive index vanishes²⁴; therefore, the corresponding bandgap is also called the zero- \bar{n} gap. At this frequency the periodic structure cannot support propagating modes, and, since the only condition for the existence of such a gap is that the volume average of the refractive index vanishes, $\bar{n} = 0$, its properties do not depend on the scaling of the structure or the polarization of the incident waves.

In previous studies it has been assumed that the LHM slabs in the LHM–RHM-layered structures were made from a homogeneous material, so that their electromag-

netic properties were described by an effective electric permittivity and an effective magnetic permeability. This is a good approximation for metal-based LHMs, as the wavelength at which these metamaterials have a negative index of refraction is much larger than the lattice constant of their periodic structure. However, inasmuch as metal-based LHMs can have large optical losses, it would be difficult to use such metamaterials to demonstrate experimentally the existence of the zero- \bar{n} gap. We demonstrate in this paper that, as an alternative to this approach, zero- \bar{n} gaps can be observed in binary PC superlattices, in which one component of the unit supercell is a PC with negative effective index of refraction. This is a nontrivial result, as at the frequency at which the zero- \bar{n} gap is formed the corresponding wavelength is only a few times larger than the periodicity of the PC, so that the effective parameters of the crystal are not well defined.

The paper is organized as follows. In Section 2 we describe the structure of our photonic superlattices. Then in Section 3 we demonstrate that, by assembling in a periodic superlattice layers of RHM and PC slabs with negative effective index of refraction, one obtains photonic structures with new optical properties, namely, structures with a zero- \bar{n} gap. In Section 4 we summarize our results.

2. DESCRIPTION OF THE PHOTONIC SUPERLATTICE

The photonic structure we consider here consists of alternating layers of materials with distinct optical properties, periodically distributed along the longitudinal axis, z . In what follows, we will consider three distinct cases, namely, both layers are made from homogeneous materials; one layer is made from a two-dimensional (2D) PC, whereas the other is a homogeneous RHM; and, finally, both layers are made from 2D PCs with different geometrical parameters. For the 2D PC we consider a hexagonal lattice of air holes in a dielectric background (see Fig. 1). The optical properties of the PC slab are fully determined by the lattice constant a ; the ratio r/a , where r

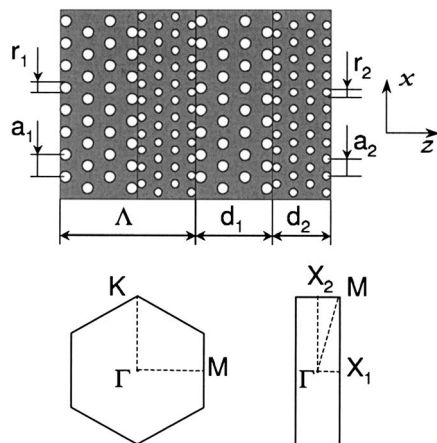


Fig. 1. Schematic design of a binary PC superlattice. The parameters $a_{1,2}$ and $r_{1,2}$ are the lattice constants and the air-hole radii, respectively, and the superlattice period is $\Lambda = d_1 + d_2$. Also shown are the first Brillouin zones of the hexagonal PC and the PC superlattice.

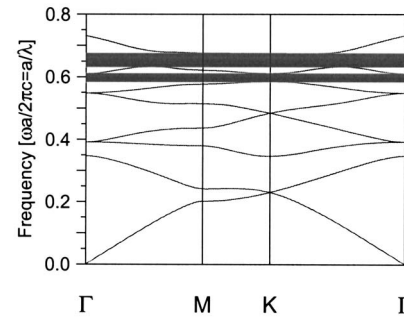


Fig. 2. PBS of the TM modes for an air-hole hexagonal PC with parameter $r/a=0.4$ and the index of refraction of the dielectric background $n=3.6$. The shadowed regions correspond to photonic bandgaps.

is the radius of the air holes; and the refractive index n of the dielectric background. Furthermore, the photonic superlattice is periodic along the longitudinal direction, with $\Lambda = d_1 + d_2$ as the corresponding spatial periodicity. Here, d_1 and d_2 are the thicknesses of the two slabs contained in the primary unit supercell. Note that the hexagonal PC and the photonic superlattice have different symmetry properties, and therefore they also have different first Brillouin zones²⁹ (see Fig. 1).

We assume that the wave vector of the plane wave incident on the superlattice lies in the xz plane and that the incident plane wave is either s polarized, with the electric field along the y axis, or p polarized, with the magnetic field oriented along the y axis. On the other hand, when describing the modes that propagate inside the superlattice we will follow the convention used in the PC-related literature, namely, that the TM (TE) modes have the only nonzero component of the electric (magnetic) field oriented along the y axis.

For the 2D PC we consider a hexagonal lattice of air holes in a dielectric background with index of refraction $n=3.6$ and structural parameter $r/a=0.4$. In this geometry, only the TM polarization provides a range of frequencies in which only one photonic band exists, so that phenomena such as multiple-beam excitation are greatly reduced, and, more importantly, this band has a negative effective index of refraction. In addition, this negative index of refraction is isotropic within a large frequency domain. Therefore, in our analysis we will consider only the TM polarization. These dispersive properties of the primary PC structure are illustrated in Fig. 2, where the photonic band structure (PBS) of the TM modes is shown. Thus, at low frequencies (first photonic band) the mode frequency increases almost linearly with the mode wave vector, which is a consequence of the fact that at large wavelengths the PC structure behaves like an effective homogeneous medium. This description changes if we consider the second band, which extends between $\bar{\omega} = 0.23$ and $\bar{\omega} = 0.347$, where $\bar{\omega} = \omega a / 2\pi c = a/\lambda$ is the normalized frequency. For this band the mode frequency decreases with the mode wave vector (anomalous dispersion), a property that leads to a negative effective index of the photonic modes in this band.^{16,17}

To illustrate this property, let us consider the wave refraction at a RHM-PC interface, for wave frequencies that belong to the second band, and compare it with the

wave refraction at a RHM–RHM interface. These processes are shown schematically in Fig. 3. Thus, in two dimensions, for an isotropic RHM the equipfrequency surface (EFS) $\omega = \omega(\mathbf{k})$ is a circle, with the corresponding group velocity $\mathbf{v}_g = \nabla_{\mathbf{k}}\omega(\mathbf{k})$ pointing outward and normal to the EFS. In contrast, in the case of a PC, at a frequency in which the dispersion is anomalous (e.g., second photonic band in Fig. 2), the group velocity points inward but again normal to the EFS. Now let us consider a plane wave that propagates in a RHM and impinges at a certain angle on a PC, as illustrated in Fig. 3, and let us assume that at the frequency of the incoming plane wave the dispersion of the PC is anomalous. Then the conservation of the component of the wave vector that is parallel to the interface determines two possible choices for the wave vector of the transmitted wave [corresponding to the intersections between the vertical dashed line in Fig. 3(a) and the EFS]. Between these two choices, only one is physically acceptable, namely, the one that ensures an energy flow from the RHM into the LHM. Hence, to select the correct direction of propagation of the transmitted wave, we use the property that in a PC the Poynting vector \mathbf{S} is oriented along the group velocity,³⁰ which, for a frequency in which the dispersion is anomalous, is perpendicular to the EFS and inwardly oriented. As a result, we observe that the refraction at the interface is negative, the Poynting vector \mathbf{S} of the transmitted wave is opposite to its wave vector, $\mathbf{S} \cdot \mathbf{k}_r < 0$, and thus the effective index n (also called phase index) defined by $|\mathbf{k}| = |n|\omega/c$ is negative. All these properties are defining characteristics of a LHM. In the case of refraction at the interface between two RHMs, the group velocity of the transmitted wave is along the wave vector so that the incident and the transmitted waves are on the opposite sides of the normal to the interface.

Inasmuch as we want to use a PC slab as the LHM component in a photonic superlattice, we performed a more detailed analysis of the dispersive properties of the primary 2D PC structure, in the frequency range in which its effective index of refraction is negative (the second band in Fig. 2). In particular, we have numerically computed the effective index of the second photonic band, for all propagation wave vectors in the first Brillouin zone of the 2D PC. The results of our calculations, summarized in Fig. 4, show that at frequencies corresponding to this pho-

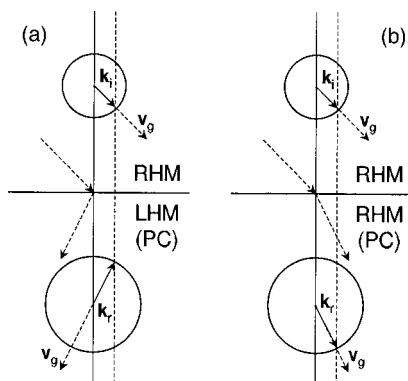


Fig. 3. Schematic representation of wave refraction (a) at the interface between a RHM and a LHM and (b) at the interface between two RHMs. The vertical dashed lines illustrate the conservation of the wave vector parallel at the interface.

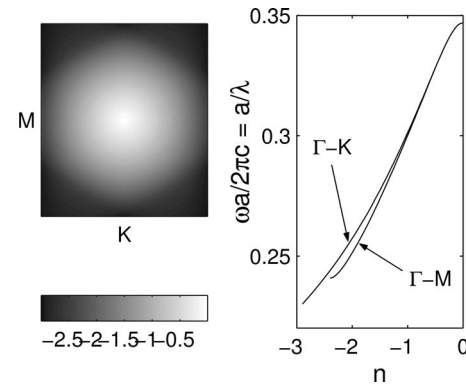


Fig. 4. Effective index of refraction of the propagating modes belonging to the second photonic band shown in Fig. 2. In the right panel, the frequency dispersion of the effective index of refraction of the modes whose wave vectors span the Γ – M and Γ – K symmetry axes.

tonic band the wave propagation in the PC is nearly isotropic, especially if the wave vectors of the Bloch modes are close to the Γ symmetry point. At these frequencies the corresponding EFSs are slightly deformed circles, whereas the EFSs that correspond to frequencies close to the bottom of the band approach an hexagonal shape. For example, for the direction of propagation along the Γ – M symmetry axis the effective index is $n = -1$ for $\bar{\omega} = 0.3$, whereas at the same frequency, but for the direction of propagation along the Γ – K symmetry axis, the effective index is $n = -1.022$. In what follows, we will demonstrate that, because of this near optical isotropy, a PC slab can be used as one of the two components in a photonic binary superlattice so as to create a zero- \bar{n} gap.

3. ZERO- \bar{n} GAP IN RHM–LHM PHOTONIC SUPERLATTICES

In this section we will demonstrate that in a photonic superlattice that contains as one of its components a PC with negative effective index of refraction one can create a photonic gap whose properties do not depend on the spatial periodicity of the superlattice or the index of refraction of its components. In contrast with the Bragg gap, this photonic gap is formed at a frequency at which the spatial average of the effective index of refraction of the superlattice vanishes. In addition, this gap is omnidirectional, provided that at the corresponding frequency the PC layers in the unit supercell are optically isotropic.

A. Superlattices of Homogeneous RHM and LHM Layers

To begin with, let us briefly discuss the case in which both layers in the unit supercell are made from homogeneous materials. Here we restrict our discussion to the case of dispersionless media and consider only periodic structures whose spatial average of the refractive index vanishes, that is $\langle n \rangle = (n_1 d_1 + n_2 d_2) / \Lambda = 0$ (the general case has been discussed in a recent study²⁵). Thus, by assuming that the electromagnetic field in the supercell is a Bloch mode, i.e., $\mathcal{F}(z + \Lambda) = \exp(ik_2 \Lambda) \mathcal{F}(z)$, one can easily derive the dispersion relation of the photonic modes³¹:

$$\cos(k_z \Lambda) = \cos \beta_1 \cos \beta_2 - \frac{1}{2} \left(\frac{p_1}{p_2} + \frac{p_2}{p_1} \right) \sin \beta_1 \sin \beta_2, \quad (1)$$

where the Bloch wave vector k_z belongs to the first Brillouin zone of the superlattice, $-\pi/\Lambda \leq k_z \leq \pi/\Lambda$. In Eq. (1) the parameters $p_{1,2}$ depend on the polarization of the Bloch mode and are given by

$$p_1 = \left(\frac{\epsilon_1}{\mu_1} \right)^{1/2} \cos \theta_1, \quad p_2 = \left(\frac{\epsilon_2}{\mu_2} \right)^{1/2} \cos \theta_2 \quad (2)$$

for *s*-polarized waves and

$$p_1 = \left(\frac{\mu_1}{\epsilon_1} \right)^{1/2} \cos \theta_1, \quad p_2 = \left(\frac{\mu_2}{\epsilon_2} \right)^{1/2} \cos \theta_2 \quad (3)$$

for *p*-polarized waves, whereas the parameters $\beta_{1,2}$ are defined as

$$\beta_1 = \frac{\omega}{c} \sqrt{\epsilon_1 \mu_1} d_1 \cos \theta_1, \quad \beta_2 = \frac{\omega}{c} \sqrt{\epsilon_2 \mu_2} d_2 \cos \theta_2. \quad (4)$$

Here, $\theta_{1,2}$ are the angles between the propagating waves in the two media and the normal to the interface between them. Since the tangent component k_x of the wave vector is the same in the two media, the angles $\theta_{1,2}$ are determined by the following expressions:

$$\cos \theta_i = \left[1 - \frac{1}{\epsilon_i \mu_i} \left(\frac{k_x c}{\omega} \right)^2 \right]^{1/2} \quad (i = 1, 2). \quad (5)$$

The dispersion properties of the superlattice are derived from Eq. (1) as follows. If for a given frequency ω and tangent component k_x of the wave vector the absolute value of the right-hand side of Eq. (1) is less than 1, then there is a real solution k_z that satisfies this equation. Therefore, at the frequency ω there exists a propagating Bloch mode with the wave vector $\mathbf{k} = (k_x, k_z)$. On the other hand, if the absolute value of the right-hand side of Eq. (1) is larger than 1, the corresponding solution k_z has a nonzero imaginary part, which means that the superlattice does not support propagating Bloch modes.

We have used this procedure to calculate the PBS of a RHM–LHM superlattice with material parameters $\epsilon_1 = 4.8$, $\mu_1 = 1$, $\epsilon_2 = -2.5$, $\mu_2 = -5$, and the thicknesses of the two layers $d_1 = f\Lambda$ and $d_2 = (1-f)\Lambda$, with $f = 0.6174$. We choose the values of these parameters such that the average index of refraction of the superlattice $\langle n \rangle = (n_1 d_1 + n_2 d_2) / \Lambda = 0$. The results of these calculations are presented in Fig. 5, where both the projected as well as the reduced band structures are shown. In both cases we considered *s* and *p* polarizations. For the sake of clarity, the results are displayed in normalized units, namely, $\omega \rightarrow \omega \Lambda / 2\pi c$, $k_x \rightarrow \kappa_x = k_x \Lambda / 2\pi$, and $k_z \rightarrow \kappa_z = k_z \Lambda / 2\pi$. These figures illustrate several phenomena, which are specific to RHM–LHM periodic structures. Thus, Fig. 5(a) shows that for small values of the tangent component κ_x the transmission through the superlattice is zero, except in certain narrow transmission bands. At the frequencies of these bands, determined by the Fabry–Perot resonance condition²⁴

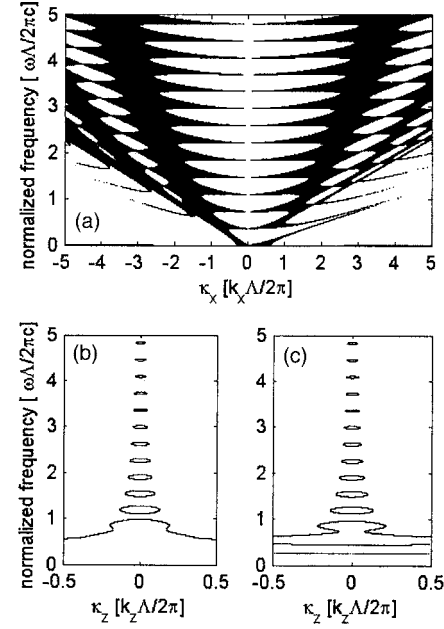


Fig. 5. (a) Projected PBS (left, *s* polarization; right, *p* polarization) of a photonic superlattice with material parameters $\epsilon_1 = 4.8$, $\mu_1 = 1$, $\epsilon_2 = -2.5$, $\mu_2 = -5$, and the thicknesses of the two layers $d_1 = f\Lambda$ and $d_2 = (1-f)\Lambda$, with $f = 0.6174$. The black (bold) regions correspond to transmission bands. Near $\kappa_x = 0$, these bands collapse to discrete states. (b), (c) The reduced PBS for *s* and *p* polarizations, calculated for $\kappa_x = 1.2$, respectively.

$$\beta_1 = m\pi \quad (m = \pm 1, \pm 2, \pm 3, \dots), \quad (6)$$

the waves, reflected at consecutive interfaces, arrive out of phase at the input facet of the superlattice. These bands narrow as κ_x decreases, collapsing to discrete states at $\kappa_x = 0$. This behavior is quite different from that of a RHM–RHM superlattice, in which case at $\kappa_x = 0$ there are a series of alternating transmission bands and Bragg gaps, equally spaced in the normalized frequency ω space. Moreover, Fig. 5 shows that, although there is a quantitative difference between the dispersion properties of the *s*- and *p*-polarized waves, qualitatively they are similar.

B. Superlattices of Homogeneous RHM and PC-Based LHM Layers

We now turn our attention to a superlattice whose supercell is made from a PC slab, with the structural parameters described in Section 2, and a homogeneous RHM slab. We consider the RHM to be dispersionless and choose the frequency of the plane wave incident on the superlattice such that the effective index of the PC is negative. Also, the orientation of the PC slab is chosen such that the *z* axis coincides with the Γ –*M* symmetry axis of the crystal and the facets of the PC slab are planes that contain the centers of the air holes. We will demonstrate that under these conditions a zero- \bar{n} gap opens at the frequency at which the spatial average of the refractive index, $\langle n \rangle$, vanishes. Note that in this case the effective refractive index of the PC depends on the frequency (see Fig. 4), and, consequently, we expect that, unlike the case

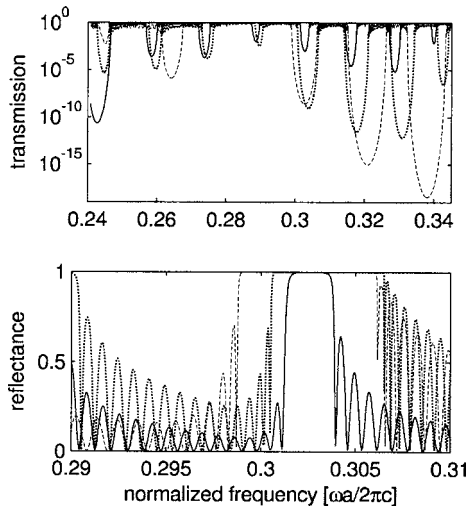


Fig. 6. Frequency dependence of transmission (upper panel) and reflectance (lower panel), computed for three different superlattices. The dashed, dotted, and solid curves correspond, respectively, to superlattices (i), (ii), and (iii) (see the text for the description of their structure).

of a RHM–LHM superlattice made from homogeneous dispersionless media, the frequency width of the gap will be finite.

To demonstrate the existence of the zero- \bar{n} gap, we have first examined the transmission and reflection properties of a stack of PC and RHM layers. We varied both the refractive index of the RHM slab as well as the thicknesses of both layers. Thus, we considered three superlattices whose unit supercells were defined as follows: (i) a PC slab containing six unit cells along the z axis, so that the thickness of the layer is $d_1 = 3\sqrt{3}a$, and a RHM with $d_2 = d_1$ and index of refraction $n_2 = 1$, i.e., vacuum; (ii) a PC slab containing eight unit cells along the z axis, so that the thickness of the layer is $d_1 = 4\sqrt{3}a$, and again a RHM with $d_2 = d_1$ and index of refraction $n_2 = 1$; and (iii) a PC slab containing eight unit cells along the z axis, so that the thickness of the layer is $d_1 = 4\sqrt{3}a$, and a RHM with the refraction index $n_2 = 2.2$ and $d_2 = d_1/n_2$. With this choice, in all three cases the spatial average of the refractive index vanishes at the frequency at which the effective index of the PC slab is $n_{PC} = n_1 = -1$, that is, for the normalized frequency $\bar{\omega} = 0.3$. Finally, in all these three cases we numerically calculated the transmission and reflection at normal incidence, for TM wave polarization (s -polarized incident wave), for a superlattice containing eight supercells. For this, we used a numerical algorithm that relates the transmission and reflection coefficients of a periodic structure to the transfer matrix associated with its unit cell, that is, the so-called transfer-matrix method (TMM).^{32–34} In all TMM calculations we used a 50×350 computational grid. As the corresponding numerical simulations are computationally demanding, we used a parallel implementation of the TMM algorithm, which was run on a computer cluster containing 18 Pentium 4 processors at 2.8 GHz.

Figure 6, which shows the frequency dependence of the transmission and reflectance of all three superlattices, illustrates the results of these numerical computations. First, the transmission spectrum of the photonic struc-

tures, computed for frequencies at which the PC has a negative effective index of refraction (see Fig. 4), shows several photonic gaps. In addition, one observes that the corresponding mid-gap frequencies of all but one photonic gap vary with the structural parameters of the superlattice, which is the familiar behavior of the Bragg gaps. However, the mid-gap frequency of the gap located near the normalized frequency $\bar{\omega} = 0.3$, at which the condition $\langle n \rangle = 0$ is satisfied, is nearly insensitive to changes in the structure of the superlattice. This analysis proves that one can use PCs as primary LHM building blocks to create photonic structures with new properties.

As in the case of RHM–LHM superlattices made of homogeneous materials, it is possible to design a superlattice with a PC-based LHM slab such that the zero- \bar{n} gap contains a narrow transmission band. This phenomenon is illustrated in Fig. 7, where we show the frequency dependence of transmission and reflectance of a superlattice containing a PC slab with six unit cells along the z axis, so that the thickness of the layer is $d_1 = 3\sqrt{3}a$, and a RHM with the refraction index $n_2 = 3.6$ and thickness $d_2 = d_1/n_2$. As in the previous cases we observe a gap around the frequency $\bar{\omega} = 0.3$, that is, the normalized frequency at which $\langle n \rangle = 0$. However, inside this transmission gap we see a sharp transmission resonance at the frequency $\bar{\omega} = 0.302$. At this frequency the effective index of refraction of the PC, for propagation along the Γ – M symmetry axis, is $n_1 = -0.96$, so that the parameter $\beta_1 = 4.02\pi$. This proves that the transmission peak at $\bar{\omega} = 0.302$ is the result of resonant Fabry–Perot wave interaction.

We have also studied the dependence of the optical properties of RHM–LHM photonic superlattices on the direction of the mode propagation inside the superlattice. In particular, we examine whether the spectral properties of the zero- \bar{n} gap are preserved when the direction of the mode propagation inside the superlattice changes. For this, we have computed the PBS of three infinite superlattices with parameters $d_1 = 3\sqrt{3}a$ (six unit cells), $n_2 = 1$, and $d_2 = d_1/n_2$; $d_1 = 4\sqrt{3}a$ (eight unit cells), $n_2 = 1$, and

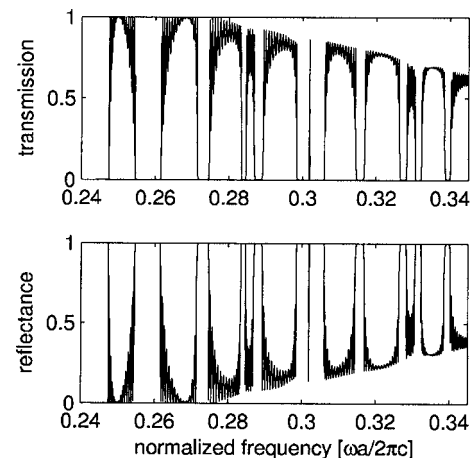


Fig. 7. Frequency dependence of transmission (upper panel) and reflectance (lower panel) computed for a superlattice containing a PC slab with six unit cells along the z axis, so that the thickness of the layer is $d_1 = 3\sqrt{3}a$, and a RHM with the refraction index $n_2 = 3.6$ and thickness $d_2 = d_1/n_2$. Note the narrow resonance at $\bar{\omega} = 0.302$.

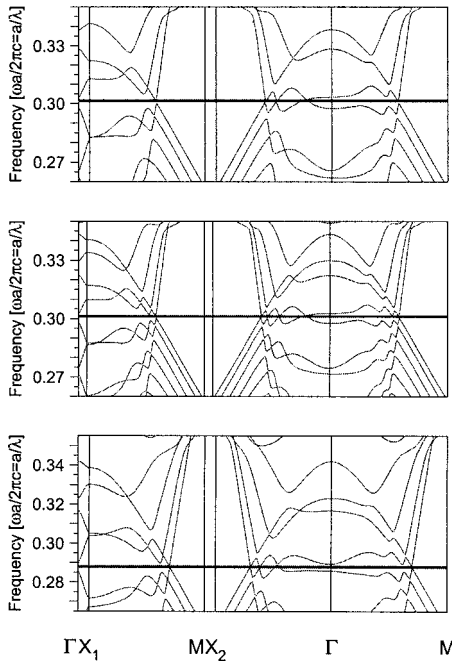


Fig. 8. From the top to the bottom panels: the PBS of three infinite superlattices with parameters $d_1=3\sqrt{3}a$ (six unit cells), $n_2=1$, and $d_2=d_1/n_2$; $d_1=4\sqrt{3}a$ (eight unit cells), $n_2=1$, and $d_2=d_1/n_2$; and $d_1=3\sqrt{3}a$ (six unit cells), $n_2=1.25$, and $d_2=d_1$. The shadowed regions correspond to photonic bandgaps.

$d_2=d_1/n_2$; and $d_1=3\sqrt{3}a$ (six unit cells), $n_2=1.25$, and $d_2=d_1$. For these values of the parameters of the superlattice $\langle n \rangle = 0$ at the frequency $\bar{\omega} = 0.3$ in the first two cases, whereas in the last case $\langle n \rangle = 0$ at the frequency $\bar{\omega} = 0.2864$. The results of these calculations are presented in Fig. 8. Note that in this figure the size of the Brillouin zone along the $\Gamma-X_1$ symmetry axis is compressed, as compared with the $\Gamma-M$ distance shown in Fig. 2, which is due to the increased size of the unit supercell along the z axis. Also, note that there is a good agreement between the position of the frequency gaps in Figs. 6 and 8 (top two panels), which were computed by using two different numerical methods, namely, the TMM and the plane-wave expansion, respectively.

One remarkable finding illustrated in Fig. 8 is that the zero- \bar{n} gap extends to all directions of propagation; i.e., it is an omnidirectional gap. This property further illustrates that the origin of this gap is not in the band folding of the photonic bands back into the first Brillouin zone, as is the case with the familiar Bragg gaps. Also, notice that for propagation directions that are off normal with respect to the PC slabs the gap narrows, an effect that is attributed to the anisotropy of the effective refractive index of the PC (see Fig. 4). Thus, for off-normal propagation the refractive index is slightly different from the refractive index for which the condition $\langle n \rangle = 0$ is satisfied, i.e., the effective index along the $\Gamma-X_1$ symmetry axis, so that the gap tends to close. Moreover, the PBS shown in the bottom panel of Fig. 8 demonstrates that the frequency of the zero- \bar{n} gap can be tuned by one's simply varying the frequency at which the condition $\langle n \rangle = 0$ is satisfied. Thus, by one's choosing $n_2 = 1.25$ and keeping $d_2 = d_1$, the average index $\langle n \rangle = 0$ for $n_1 = n_{PC} = -1.25$, that is,

at the frequency $\bar{\omega} = 0.2864$ (see Fig. 4). This value is consistent with the frequency gap shown in the bottom panel in Fig. 8, whose spectral domain extends between $\bar{\omega} = 0.2859$ and $\bar{\omega} = 0.2894$.

C. Superlattices of PC-Based RHM and LHM Layers

To conclude this section, we will show that a zero- \bar{n} photonic gap can be produced by a superlattice in which both components of the unit supercell are made from PC slabs. For this, the geometrical parameters of the two PC domains must be chosen such that at a certain frequency one PC has a positive effective index of refraction, whereas the effective index of the other one is negative. In addition, at this frequency, the spatial average of these effective indices must be zero. In what follows, we will illustrate these ideas by a specific example. Thus, let us consider that the first PC in the supercell is described by the parameters $a_1 = a$, $r_1/a_1 = 0.4$ and the background index $n = 3.6$, i.e., the previously considered PC. As the second component we consider a PC with parameters $a_2 = a_1/2$, $r_2/a_2 = 0.5$ and with the same background index $n = 3.6$. Finally, we choose the thicknesses of the two PC slabs to be $d_1 = 3\sqrt{3}a_1$ and $d_2 = 6\sqrt{3}a_2$, i.e., $d_1 = d_2$. We choose the PC slabs to be a few lattice constants thick, that is, large enough for the photonic bands to form.

The PBS of the superlattice, computed for a frequency domain in which the first PC component has negative effective index of refraction is presented in Fig. 9. Note that the frequency in this figure is normalized by using the parameters of the first PC so that, by using the scaling properties of the frequencies of the Bloch modes in a PC, we can see that these frequencies belong to the first band of the second PC, that is, a band with positive effective index of refraction. Furthermore, we have numerically calculated the effective index of refraction of this first band; these calculations show that, for direction of propagation along the $\Gamma-X_1$ symmetry axis, at the frequency $\bar{\omega} = 0.2855$ (marked in Fig. 9 by a dashed line), the effective indices of refraction of the two PC slabs are $n_1 = -n_2 = -1.27$. As the two PC slabs in the unit supercell have the same thickness, the average index of refraction at the frequency $\bar{\omega}$ is $\langle n \rangle = (n_1 d_1 + n_2 d_2) / \Lambda = 0$. Therefore, the nearly complete bandgap seen in Fig. 9, at the frequency $\bar{\omega}$, represents a zero- \bar{n} photonic gap. Note that this zero- \bar{n} photonic gap is not a complete bandgap because of the small optical anisotropy of the two PC slabs.

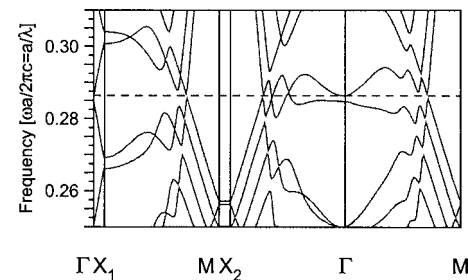


Fig. 9. PBS of a superlattice with parameters $a_1 = a$, $r_1/a_1 = 0.4$, $d_1 = 3\sqrt{3}a_1$, and the background index $n = 3.6$ for the first PC component and $a_2 = a_1/2$, $r_2/a_2 = 0.5$, $d_2 = 6\sqrt{3}a_2$, and background index $n = 3.6$ for the second PC component. The horizontal line corresponds to the frequency at which $\langle n \rangle = 0$.

4. CONCLUSIONS

In conclusion, we have demonstrated that a periodic superlattice whose unit supercell contains a PC slab with negative effective index of refraction and either a homogeneous slab of RHM or a PC slab with positive effective index of refraction has transmission properties that cannot be achieved by using only RHM-based Bragg photonic structures. In particular, we have shown that, under certain conditions that can readily be satisfied in common experimental setups, the superlattices introduced here possess a type of photonic gap with unusual and potentially useful properties. This photonic gap opens at frequencies at which the spatial average of the refractive index of the superlattice vanishes, and therefore, as long as this condition is satisfied, the gap is insensitive to periodicity of the structure, angle of incidence onto the structure, material parameters, and, possibly, structural disorder.

We stress that, although our analysis considered only 2D PCs, it can be readily extended to structures that are easy to fabricate, such as 2D PC slab waveguides. In this case, one only has to employ the effective index of the guided modes of the slab waveguide; the rest of the analysis remaining valid. In particular, for slab waveguides with small refraction index contrast, the reduction of the 3D problem to a 2D one, by using an effective index of refraction, leads to accurate results. Therefore, InP-GaInAsP-InP or silicon-on-insulator material platforms can be employed to fabricate the photonic structures discussed here. Alternatively, it may also be possible to use metal-based LHMs in a vertical thin-film stack, which is alternated with a RHM dielectric. The metal-based LHMs in this case can be conveniently fabricated using interferometric lithography⁹; in this case, particular care has to be taken regarding the total optical loss of such a structure. The availability of such structures would open up the possibility of investigating their potential use in new devices such as highly directive sources, wavefront converters, or delay lines with zero phase difference between the input and the output ports.^{35,36}

ACKNOWLEDGMENTS

This work has been supported by the Air Force Office of Scientific Research grant CU02630301, and also in part by the University of New Mexico Defense Advanced Research Projects Agency Optocenter. The computer simulation time and cluster work was supported by the Brown University Optocenter (BROWNU-1119-24596).

Corresponding author N. C. Panoiu can be reached by e-mail at panoiu@cumsl.msl.columbia.edu.

REFERENCES

1. D. R. Smith, W. J. Padilla, D. C. Vier, S. C. Nemat-Nasser, and S. Schultz, "Composite medium with simultaneously negative permeability and permittivity," *Phys. Rev. Lett.* **84**, 4184–4187 (2000).
2. R. A. Shelby, D. R. Smith, S. C. Nemat-Nasser, and S. Schultz, "Microwave transmission through a two-dimensional, isotropic, left-handed metamaterial," *Appl. Phys. Lett.* **78**, 489–491 (2001).
3. R. A. Shelby, D. R. Smith, and S. Schultz, "Experimental verification of a negative index of refraction," *Science* **292**, 77–79 (2001).
4. V. G. Veselago, "The electrodynamics of substances with simultaneously negative values of ϵ and μ ," *Usp. Fiz. Nauk* **92**, 517–526 (1964) [*Sov. Phys. Usp.* **10**, 509–514 (1968)].
5. J. B. Pendry, A. J. Holden, W. J. Stewart, and I. Youngs, "Extremely low frequency plasmons in metallic mesostructures," *Phys. Rev. Lett.* **76**, 4773–4776 (1996).
6. J. B. Pendry, A. J. Holden, D. J. Robbins, and W. J. Stewart, "Low frequency plasmons in thin-wire structures," *J. Phys. Condens. Matter* **10**, 4785–4809 (1998).
7. J. B. Pendry, A. J. Holden, D. J. Robbins, and W. J. Stewart, "Magnetism from conductors and enhanced nonlinear phenomena," *IEEE Trans. Microwave Theory Tech.* **47**, 2075–2084 (1999).
8. V. A. Podolskiy, A. K. Sarychev, and V. M. Shalaev, "Plasmon modes in metal nanowires and left-handed materials," *J. Nonlinear Opt. Phys. Mater.* **11**, 65–74 (2002).
9. S. Zhang, W. Fan, N. C. Panoiu, K. J. Malloy, R. M. Osgood, and S. R. J. Brueck, "Demonstration of near-infrared negative-index metamaterials," *Phys. Rev. Lett.* **95**, 137404 (2005).
10. J. B. Pendry, "Negative refraction makes a perfect lens," *Phys. Rev. Lett.* **85**, 3966–3969 (2000).
11. D. O. S. Melville and R. J. Blaikie, "Super-resolution imaging through a planar silver layer," *Opt. Express* **13**, 2127–2134 (2005).
12. N. Fang, H. Lee, C. Sun, and X. Zhang, "Sub-diffraction-limited optical imaging with a silver superlens," *Science* **308**, 534–537 (2005).
13. N. C. Panoiu and R. M. Osgood, "Influence of the dispersive properties of metals on the transmission characteristics of left-handed materials," *Phys. Rev. E* **68**, 016611 (2003).
14. N. C. Panoiu and R. M. Osgood, "Numerical investigation of negative refractive index metamaterials at infrared and optical frequencies," *Opt. Commun.* **223**, 331–337 (2003).
15. S. Zhang, W. Fan, K. J. Malloy, S. R. J. Brueck, N. C. Panoiu, and R. M. Osgood, "Near-infrared double negative metamaterials," *Opt. Express* **13**, 4922–4930 (2005).
16. M. Notomi, "Theory of light propagation in strongly modulated photonic crystals: refractionlike behavior in the vicinity of the photonic band gap," *Phys. Rev. B* **62**, 10696–10705 (2000).
17. M. Notomi, "Negative refraction in photonic crystals," *Opt. Quantum Electron.* **34**, 133–143 (2002).
18. B. Gralak, S. Enoch, and G. Tayeb, "Anomalous refractive properties of photonic crystals," *J. Opt. Soc. Am. A* **17**, 1012–1020 (2000).
19. S. Foteinopoulou, E. N. Economou, and C. M. Soukoulis, "Refraction in media with a negative refractive index," *Phys. Rev. Lett.* **90**, 107402 (2003).
20. A. Berrier, M. Mulot, M. Swillo, M. Qiu, L. Thylen, A. Talneau, and S. Anand, "Negative refraction at infrared wavelengths in a two-dimensional photonic crystal," *Phys. Rev. Lett.* **93**, 073902 (2004).
21. P. V. Parimi, W. T. Lu, P. Vodo, and S. Sridhar, "Imaging by flat lens using negative refraction," *Nature* **426**, 404 (2003).
22. C. Luo, S. G. Johnson, J. D. Joannopoulos, and J. B. Pendry, "Subwavelength imaging in photonic crystals," *Phys. Rev. B* **68**, 045115 (2003).
23. E. Cubukcu, K. Aydin, E. Ozbay, S. Foteinopoulou, and C. M. Soukoulis, "Subwavelength resolution in a two-dimensional photonic-crystal-based superlens," *Phys. Rev. Lett.* **91**, 207401 (2003).
24. J. Li, L. Zhou, C. T. Chan, and P. Sheng, "Photonic band gap from a stack of positive and negative index materials," *Phys. Rev. Lett.* **90**, 083901 (2003).
25. D. Bria, B. Djafari-Rouhani, A. Akjouj, L. Dobrzynski, J. P. Vigneron, E. H. El Boudouti, and A. Nougaoui, "Band structure and omnidirectional photonic band gap in lamellar structures with left-handed materials," *Phys. Rev. E* **69**, 066613 (2004).
26. H. Jiang, H. Chen, H. Li, Y. Zhang, and S. Zhu,

- “Omnidirectional gap and defect mode of one-dimensional photonic crystals containing negative-index materials,” *Appl. Phys. Lett.* **83**, 5386–5388 (2003).
27. L. Wu, S. He, and L. Chen, “On unusual narrow transmission bands for a multilayered periodic structure containing left-handed materials,” *Opt. Express* **11**, 1283–1290 (2003).
28. I. V. Shadrivov, A. A. Sukhorukov, and Y. S. Kivshar, “Beam shaping by a periodic structure with negative refraction,” *Appl. Phys. Lett.* **82**, 3820–3822 (2003).
29. W. Park and C. J. Summers, “Optical properties of superlattice photonic crystal waveguides,” *Appl. Phys. Lett.* **84**, 2013–2015 (2004).
30. K. Sakoda, *Optical Properties of Photonic Crystals* (Springer-Verlag, 2001).
31. M. Born and E. Wolf, *Principles of Optics* (Pergamon, 1983).
32. J. B. Pendry and A. MacKinnon, “Calculation of photon dispersion relations,” *Phys. Rev. Lett.* **69**, 2772–2775 (1992).
33. J. B. Pendry, “Photonic band structures,” *J. Mod. Opt.* **41**, 209–229 (1994).
34. P. M. Bell, J. B. Pendry, L. M. Moreno, and A. J. Ward, “A program for calculating photonic band structures and transmission coefficients of complex structures,” *Comput. Phys. Commun.* **85**, 306–322 (1995).
35. S. Enoch, G. Tayeb, P. Sabouroux, N. Guerin, and P. Vincent, “A metamaterial for directive emission,” *Phys. Rev. Lett.* **89**, 213902 (2002).
36. R. W. Ziolkowski, “Propagation in and scattering from a matched metamaterial having a zero index of refraction,” *Phys. Rev. E* **70**, 046608 (2004).